Novel Insights into the Aortic Mechanical Properties of Mice Modeling Hereditary Aortic Diseases

Nicolo Dubacher[1,2] Kaori Sugiyama[3,4] Jeffrey D. Smith[5] Vanessa Nussbaumer[1] Máté Csonka[1,6] Szilamér Ferenczi[7] Krisztina J. Kovács[7] Sylvan M. Caspar[1] Lisa Lamberti[1] Janine Meienberg[1] Hiromi Yanagisawa[4,*] Mary B. Sheppard[8,9,*] Gabor Matyas[1,10,*]

[1] Center for Cardiovascular Genetics and Gene Diagnostics, Swiss Foundation for People with Rare Diseases, Schlieren-Zurich, Switzerland
[2] Translational Cardiovascular Technologies, Department of Health Sciences, ETH Zurich, Zurich, Switzerland
[3] Institute for Advanced Research of Biosystem Dynamics, Research Institute for Science and Engineering, Waseda University, Tokyo, Japan
[4] Life Science Center for Survival Dynamics, Tsukuba Advanced Research Alliance, University of Tsukuba, Tsukuba, Japan
[5] Saha Cardiovascular Research Center, University of Kentucky, Lexington, Kentucky, United States
[6] Heart and Vascular Center, Semmelweis University, Budapest, Hungary
[7] Laboratory of Molecular Neuroendocrinology, Institute of Experimental Medicine, Budapest, Hungary
[8] Department of Family and Community Medicine, University of Kentucky, Lexington, Kentucky, United States
[9] Saha Aortic Center, University of Kentucky, Lexington, Kentucky, United States
[10] Zurich Center for Integrative Human Physiology, University of Zurich, Zurich, Switzerland

Address for correspondence Gabor Matyas, PhD, Center for Cardiovascular Genetics and Gene Diagnostics, Swiss Foundation for People with Rare Diseases, Wagistrasse 25, 8952 Schlieren-Zurich, Switzerland (e-mail: matyas@genetikzentrum.ch).

Thromb Haemost

Abstract

Objective Hereditary aortic diseases (hADs) increase the risk of aortic dissections and ruptures. Recently, we have established an objective approach to measure the rupture force of the murine aorta, thereby explaining the outcomes of clinical studies and assessing the added value of approved drugs in vascular Ehlers–Danlos syndrome (vEDS). Here, we applied our approach to six additional mouse hAD models.

Material and Methods We used two mouse models (*Fbn1*^{C1041G} and *Fbn1*^{mgR}) of Marfan syndrome (MFS) as well as one smooth-muscle-cell-specific knockout (SMKO) of *Efemp2* and three CRISPR/Cas9-engineered knock-in models (*Ltbp1*, *Mfap4*, and *Timp1*). One of the two MFS models was subjected to 4-week-long losartan treatment. Per mouse, three rings of the thoracic aorta were prepared, mounted on a tissue puller, and uniaxially stretched until rupture.

Results The aortic rupture force of the SMKO and both MFS models was significantly lower compared with wild-type mice but in both MFS models higher than in mice modeling vEDS. In contrast, the *Ltbp1*, *Mfap4*, and *Timp1* knock-in models presented no impaired aortic integrity. As expected, losartan treatment reduced aneurysm formation but surprisingly had no impact on the aortic rupture force of our MFS mice.

Keywords
- aortic aneurysms
- dissections
- rupture
- biomechanical integrity
- Efemp2
- Fbn1
- Marfan syndrome

* *These authors are joint senior authors.*

received
January 3, 2024
accepted after revision
May 23, 2024

DOI https://doi.org/10.1055/s-0044-1787957.
ISSN 0340-6245.

Georg Thieme Verlag KG, Rüdigerstraße 14, 70469 Stuttgart, Germany

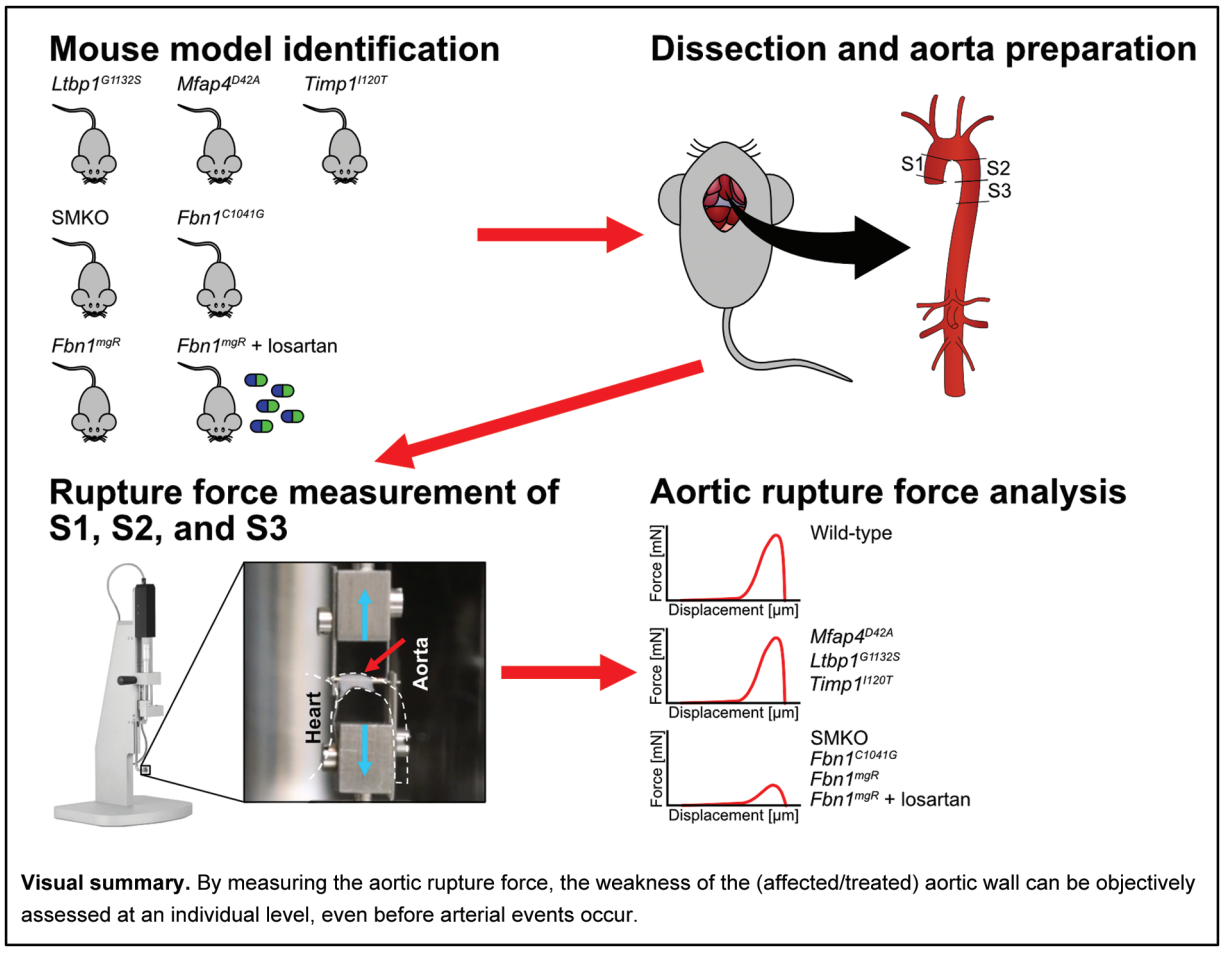

Visual summary. By measuring the aortic rupture force, the weakness of the (affected/treated) aortic wall can be objectively assessed at an individual level, even before arterial events occur.

Conclusion Our read-out system can characterize the aortic biomechanical integrity of mice modeling not only vEDS but also related hADs, allowing the aortic-rupture-force-focused comparison of mouse models. Furthermore, aneurysm progression alone may not be a sufficient read-out for aortic rupture, as antihypertensive drugs reducing aortic dilatation might not strengthen the weakened aortic wall. Our results may enable identification of improved medical therapies of hADs.

Hereditary aortic diseases (hADs) with life-threatening aneurysms and dissections are associated with high morbidity and mortality and are the cause for up to approximately 2% of all deaths in the Western world.[1] Syndromic and nonsyndromic forms of hADs are rare (i.e., prevalence <1:2,000) but several types have been identified so far. Despite considerable phenotypic similarity, disease management can profoundly differ depending on the causative gene, requiring molecular genetic testing.[2,3] The advent of high-throughput sequencing has enabled genetic data generation at hitherto unprecedented scale, allowing for novel insights into the molecular etiology of hereditary aortopathies but requiring a high level of expertise for appropriate data analysis and variant interpretation.[4] Currently, at least 50 genes have been associated with hereditary thoracic aortic aneurysms (TAAs) and classified based on the strength of association.[5] However, these genes cannot explain all the cases of heritable TAAs, suggesting the presence of additional causative genes for hADs.[6]

Changes in the structural components of the extracellular matrix (ECM) as well as in chemical and mechanical stimuli can influence the molecular signaling pathways that regulate aortic wall homeostasis. Accordingly, hAD-causing sequence variants (mutations) can affect proper ECM organization, thereby directly impacting the mechanical properties of the aorta as well as the mechanoregulation of vascular smooth muscle cells and their ability to sense matrix-mediated mechanical stimuli.[7] This can result in impaired aortic integrity and mechanical dysfunction causing progressive weakening of the aortic wall, ultimately leading to arterial dissection and/or rupture.[8] The mechanical properties of the thoracic aorta can be derived from in vivo imaging parameters such as aortic-wall distensibility and local pulse wave velocity or studied directly in ex vivo aortic samples.[9–11] In humans, however, studies

assessing the clinically relevant parameter of aortic rupture (with or without aneurysm/dissection) in hAD are significantly limited. Thus, nonhuman models harboring disease-causing variants in hAD-associated gene(s) provide a valuable alternative, when combined with an appropriate read-out at individual level.

Recently, we have established an objective approach to measure the aortic rupture force (maximum tensile force) of uniaxially stretched murine thoracic aortic rings as a read-out for the biomechanical integrity of the aorta.[12] We have previously used this approach to clarify whether or not antihypertensive drugs can also strengthen the thoracic aorta (i.e., increase rupture force), thereby showing that celiprolol, a third-generation β-blocker, but not losartan, an angiotensin-II-receptor-type-1 (AGTR1) inhibitor, can improve the biomechanical integrity of the aortic wall (i.e., beyond the celiprolol's expected effect of slowing heart rate and lowering blood pressure).[12] Accordingly, our approach provided a possible explanation for the previous outcomes of clinical and retrospective studies in vascular Ehlers–Danlos syndrome (vEDS; OMIM #130050).[13–15] This added value of celiprolol, however, cannot simply be extrapolated to other β-blockers, as we have previously demonstrated for bisoprolol.[16]

Here, we applied our established read-out approach[12] to measure the aortic rupture force in six additional mouse hAD models and compared their aortic rupture force with that of vEDS mice: (1) we used the two most widely investigated mouse models of Marfan syndrome (MFS; OMIM #154700) (*Fbn1*^{C1041G} and *Fbn1*^{mgR}),[17–19] a rare autosomal-dominant disease with severe cardiovascular manifestations, such as TAAs predisposing to aortic dissection and rupture, caused by mutations in the gene encoding fibrillin-1 (*FBN1* in humans, *Fbn1* in mice).[20] In one of the two mouse MFS models (*Fbn1*^{mgR}), we also aimed to clarify whether or not the frequently prescribed losartan, which has been shown to slow down aneurysm progression in mouse models as well as humans with MFS,[21–25] also strengthens the potentially weakened thoracic aorta. (2) Furthermore, we assessed the aortic rupture force in an *Efemp2* (encoding fibulin-4 [Fbln4]) smooth-muscle-specific knockout (SMKO) model recapitulating key vascular phenotypic features (aortic aneurysms and arterial tortuosity)[26] of the autosomal-recessive connective tissue disorder cutis laxa type 1B (OMIM #614437).[27,28] (3) Moreover, we used three novel CRISPR/Cas9-engineered knock-in models (*Ltbp1*^{G1132S}, *Mfap4*^{D42A}, *Timp1*^{I120T}) to assess the causality of human-equivalent variants in hAD candidate genes detected by whole-genome sequencing (WGS).[6]

Methods

Mouse Strains

In this study, multiple mouse strains were used. An overview can be found in the Major Resources Table in the **Supplemental Material** (available in the online version). Wild-type mice are referred to as $^{+/+}$. Mice of both sexes were used for the mouse models and losartan treatment, and measurements of aortic rupture force were performed blinded for genotype and treatment.

Fbn1^{C1041G} and *Fbn1*^{mgR} Mouse Models

For the *Fbn1*^{C1041G} mouse model (C57BL/6J background), 10-week-old heterozygous (*Fbn1*$^{+/C1041G}$, $n = 10$) and wild-type (*Fbn1*$^{+/+}$, $n = 10$) mice were ordered in frozen condition from Jackson Laboratory (JAX stock #012885, Bar Harbor, Maine, United States). Tail biopsies were taken to confirm the genotypes of delivered mice, for which DNA extraction, polymerase chain reaction (PCR), and subsequent Sanger sequencing were performed as previously described.[12,17]

Fbn1^{mgR} mice (C57BL/6J background) were bred and maintained on a 14-/10-hour light/dark cycle receiving standard rodent chow and water *ad libitum*. Mice were genotyped as described previously.[18] In addition, 4-week-old homozygous (*Fbn1*$^{mgR/mgR}$, $n = 12$) and wild-type (*Fbn1*$^{+/+}$, $n = 10$) mice were randomly assigned and treated for 4 weeks with losartan dissolved in drinking water (prepared weekly from powder and protected from light by wrapping drinking bottles in aluminum foil) at a concentration of 600 mg/L[21] (LTK Labs, St. Paul, Minnesota, United States, approximately 180 mg/kg bodyweight per day); age-matched, untreated *Fbn1*$^{mgR/mgR}$ ($n = 17$) and *Fbn1*$^{+/+}$ ($n = 10$) littermates receiving normal drinking water served as controls. Animals were weighed at the beginning and at the end of the treatment and water consumption was monitored regularly to ensure that control and treated mice drank comparable quantities. At the end of the treatment, mice were euthanized using CO_2 and subsequently frozen. Animal experimentation and maintenance were conducted in the University of Kentucky Division of Laboratory Animal Sciences facility in Lexington, Kentucky, and approved by the University of Kentucky IACUC (approval reference number: 2016–2437) in line with the local guidelines.

Efemp2 SMKO Model

Efemp2$^{loxP/KO}$;*SM22-Cre*$^{Tg/Tg}$ (SMKO) and wild-type littermates (wild-type for *Efemp2* but containing the SM22α-Cre transgene, *Efemp2*$^{+/+}$;*SM22-Cre*$^{Tg/Tg}$) with a mixed genetic background (C57BL/6J; 129SvEv) were bred and maintained on a 12-hour light/dark cycle receiving standard rodent chow and water *ad libitum*. Genotyping was performed as previously described.[26] Wild-type ($n = 11$) and SMKO ($n = 11$) littermates were euthanized with CO_2 at 8 weeks of age and subsequently frozen. Animal experimentation and maintenance were conducted in the Laboratory Animal Resource Center at the University of Tsukuba, Tsukuba, Japan, and approved by the Institutional Animal Experiment Committee of the University of Tsukuba, Japan (approval reference number: 21–108).

CRISPR/Cas9-Engineered Mouse Models

Three CRISPR/Cas9 knock-in mouse models (*Ltbp1*^{emG1132S}, *Mfap4*^{emD42A}, and *Timp1*^{emI120T}) were generated on the C57BL/6NJ background by Cyagen (Santa Clara, California, United States), thereby introducing human-equivalent sequence variants detected in our WGS cohort of hAD patients (GRCm38/mm10 chr17(Ltbp1):g.75,315,062G > A, chr11 (Mfap4):g.61,486,071A > C, and chrX(Timp1):g.20,873,395T > C, modeling human variants *LTBP1* NM_206943.4: c.3418G

>A p.(Gly1140Ser), *MFAP4* NM_001198695.2: c.191A>C p.(Asp64Ala), and *TIMP1* NM_003254.3: c.356T>C p.(Ile119Thr), respectively). Founder mice of the three strains were bred and maintained on a 12-hour light/dark cycle receiving standard rodent chow and water *ad libitum*. The genotype was determined after weaning at the age of 4 weeks by PCR and subsequent Sanger sequencing using genomic DNA extracted of ear biopsies as previously described.[12] Primers used for PCR and sequencing are listed in ►**Supplementary Table S1** (available in the online version). One-year-old heterozygous ($Ltbp1^{+/G1132S}$, $n=10$; $Mfap4^{+/D42A}$, $n=10$; $Timp1^{+/I120T}$, $n=7$), homozygous ($Ltbp1^{G1132S/G1132S}$, $n=10$; $Mfap4^{D42A/D42A}$, $n=8$; $Timp1^{I120T/I120T}$, $n=5$), and hemizygous ($Timp1^{0/I120T}$, $n=9$) mice as well as age-matched wild-type littermates serving as controls ($Ltbp1^{+/+}$, $n=10$; $Mfap4^{+/+}$, $n=9$; $Timp1^{+/+}$, $n=8$) were euthanized with CO_2 and subsequently frozen (cf. 1-year-old mice were used to be able to detect any late-onset effects of the variants). Animal experimentation and maintenance were conducted in the facility of the Laboratory Animal Services Center of the University of Zurich, Schlieren-Zurich, Switzerland, in accordance with institutional and local guidelines (approval reference number: ZH107/17, Zurich, Switzerland) conforming to the EU Directive 2010/63/EU for animal experiments.

Aortic Rupture Force Measurements

All euthanized mice were kept in a frozen state (enabling storage over a longer period of time) and thawed immediately before the aortic rupture force was measured. For all mouse models, the maximum tensile force at rupture (in mN) of three uniaxially stretched 1.5-mm thoracic aortic rings/segments (segment S1, ascending aorta, after heart; segment S2, descending aorta, after aortic arch; segment S3, descending aorta, adjacent to S2; cf. graphical abstract and note that S1–S3 are ring-shaped) per mouse was measured and relative rupture force was calculated by setting the arithmetic mean of the respective wild-type S1 to 100% as previously described.[12] The measured aortic segments were damaged by rupture and were therefore discarded after the measurements. The stretching positions of the tissue puller until both 5 mN (load-free aortic diameter) and maximum force (rupture of aortic segment) were determined (in µm) as moved distance of the mounting pins during stretching. Mice were randomized and all measurements were performed blinded to genotype and losartan treatment for the investigator.

Statistical Analyses

For arithmetic means, 95% confidence intervals (CIs) were calculated using two-tailed critical values of *t*-distribution (vassarstats.net/conf_mean.html). For means with non- or slightly (<2% of means) overlapping 95% CIs compared in the text, two-tailed *p*-values were calculated by two-sample *t*-test (equal sample variances according to *F*-test) or Welch's *t*-test (unequal sample variances according to *F*-test), assuming normal distribution of independent samples (vassarstats.net/tu.html). Valid outliers were identified by manual evaluation of data with >2 standard deviations and excluded from the study in justified cases, such as damaged aortic segments. For proportions, 95% CIs were calculated with continuity correction (vassarstats.net/prop1.html). For additional information, see the **Supplemental Material** (available in the online version).

Results

$Fbn1^{C1041G}$ Mouse Model

Compared with $Fbn1^{+/+}$ mice, the aortic rupture force of $Fbn1^{+/C1041G}$ mice was significantly decreased in all three aortic segments (S1, S2, and S3) (►**Fig. 1A**; ►**Supplementary Table S2**, available in the online version). No significant difference in stretch was detected for any of the three aortic segments of 10-week-old $Fbn1^{+/+}$ and $Fbn1^{+/C1041G}$ mice

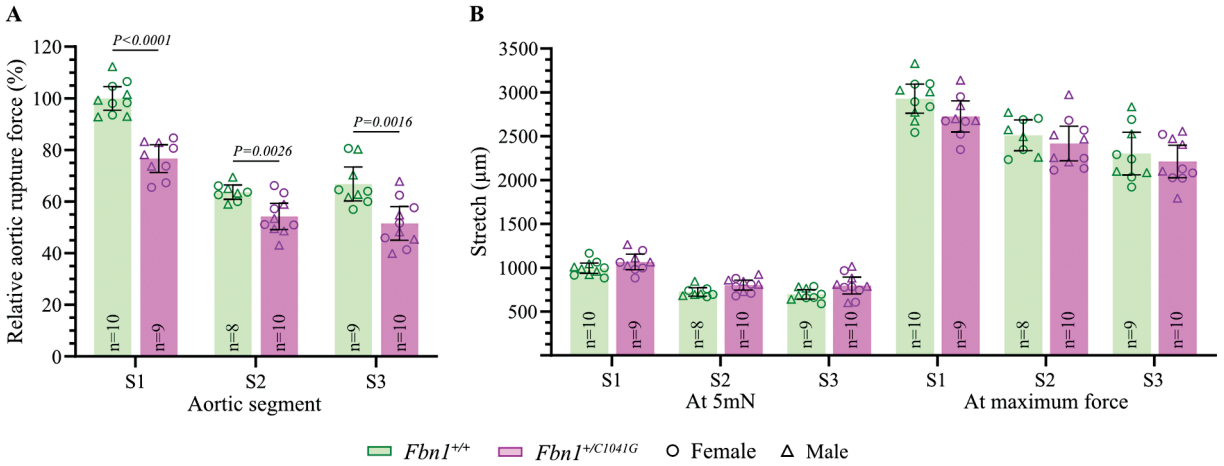

Fig. 1 Aortic parameters of the $Fbn1^{C1041G}$ mouse model. (**A**) Relative aortic rupture force (%) of three aortic segments (S1–S3) of 10-week-old $Fbn1^{+/+}$ and $Fbn1^{+/C1041G}$ mice. (**B**) Stretch (in µm) of aortic segments at 5 mN (load-free aortic diameter) and maximum force of 10-week-old $Fbn1^{+/+}$ and $Fbn1^{+/C1041G}$ mice. Bars represent arithmetic means and error bars indicate 95% confidence intervals (95% CIs). The sample size (*n*) is displayed. For mean values with non- or slightly overlapping 95% CIs compared in text, two-tailed *p*-values of unpaired *t*-tests are shown (applies to panel A only).

when stretch was measured at 5 mN or maximum force (►**Fig. 1B**; ►**Supplementary Tables S3** and **S4**, available in the online version). The relative aortic rupture force and stretch values of *Fbn1*$^{+/+}$ and *Fbn1*$^{+/C1041G}$ mice were comparable in both sexes (►**Supplementary Figs. S1** and **S3A**, available in the online version).

Fbn1^{mgR} Mouse Model

During 4 weeks of losartan treatment started at 4 weeks of age, the mortality rate of treated *Fbn1*$^{mgR/mgR}$ mice (8.3% [95% CI: 0.4–40.2%]) was not significantly lower than that of untreated *Fbn1*$^{mgR/mgR}$ mice (11.8% [95% CI: 2.1–37.7%]), but no wild-type littermate mice died (►**Fig. 2A**). On average, males were heavier than females,[29] but body weight did not differ significantly between untreated and treated mice of the same sex and genotype either before initiation of treatment (at 4 weeks of age) or after 4 weeks of treatment (at 8 weeks of age) (►**Fig. 2B**).

Compared with untreated *Fbn1*$^{+/+}$ mice, the aortic rupture force was significantly decreased in all three aortic segments of both untreated and losartan-treated *Fbn1*$^{mgR/mgR}$ mice, also revealing that losartan did not strengthen the weakened aortic wall of *Fbn1*$^{mgR/mgR}$ mice (►**Fig. 3A**; ►**Supplementary Figs. S2** and **S3B**, available in the online version; ►**Supplementary Table S5**, available in the online version). The stretch of aortic segment S1 at both 5 mN and maximum force was significantly increased in untreated *Fbn1*$^{mgR/mgR}$ mice compared with untreated *Fbn1*$^{+/+}$ mice, which was more pronounced in males (►**Fig. 3B**; ►**Supplementary Tables S6** and **S7,** available in the online version). While losartan treatment of *Fbn1*$^{+/+}$ mice had no effect on S1 stretch (►**Fig. 3B**; ►**Supplementary Tables S6** and **S7,** available in the online version), losartan treatment of *Fbn1*$^{mgR/mgR}$ mice reduced S1 stretch at both 5 mN and maximum force regardless of sex (►**Fig. 3B**; ►**Supplementary Tables S6** and **S7**, available in the online version); in S2 and S3 there were no considerable differences in stretch, so these data are not shown). Thus, our data demonstrate that losartan did not significantly alter S1–S3 rupture force but did affect S1 stretch in *Fbn1*$^{mgR/mgR}$ mice modeling MFS.

Efemp2 SMKO Mouse Model

Compared with wild-type mice, our measurements showed significantly reduced relative aortic rupture force in the ascending thoracic aorta (S1) but no difference in the descending aorta (S2 and S3) of SMKO mice (►**Fig. 4A**; ►**Supplementary Table S8**, available in the online version). Furthermore, in SMKO mice the stretch at both 5 mN and maximum force was significantly higher in the ascending aorta (S1) but significantly lower in the descending aorta (S3) at maximum force (►**Fig. 4B**; ►**Supplementary Tables S9** and **S10,** available in the online version). Increased stretch of S1 at 5 mN was associated with a lower rupture force (►**Supplementary Fig. S3C**, available in the online version).

Ltbp1, *Mfap4*, and *Timp1* CRISPR/Cas9 Knock-In Mouse Models

During the 1-year period of aging, no *Ltbp1*, *Mfap4*, or *Timp1* CRISPR/Cas9 knock-in mice died due to aortic rupture.

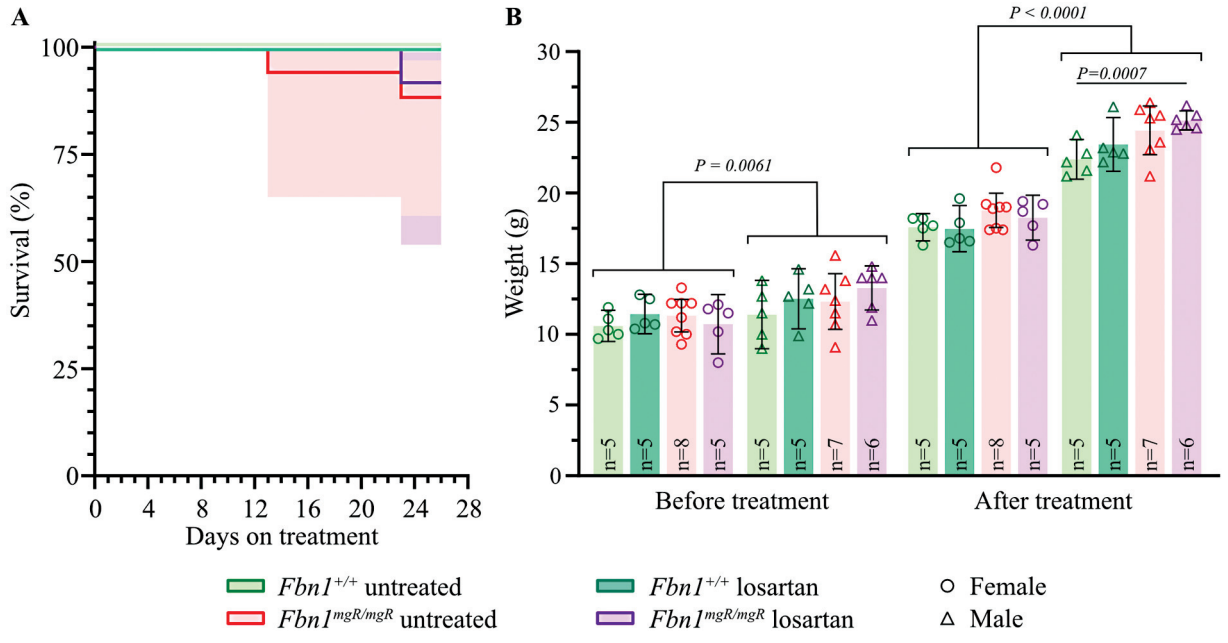

Fig. 2 Survival and bodyweight of the *Fbn1*^{mgR} mouse model treated with the AGTR1-inhibitor losartan. (**A**) Kaplan–Meier curve for the survival of untreated *Fbn1*$^{+/+}$ mice ($n = 10$) and *Fbn1*$^{mgR/mgR}$ mice ($n = 17$), and *Fbn1*$^{+/+}$ ($n = 10$) and *Fbn1*$^{mgR/mgR}$ ($n = 12$) mice receiving losartan between the age of 4 and 8 weeks. Note that the survival curve of losartan-treated *Fbn1*$^{+/+}$ mice is masked by that of untreated *Fbn1*$^{+/+}$ mice. 95% confidence intervals (shaded areas) are shown for *Fbn1*$^{mgR/mgR}$ mice with survivals differing from 100%. (**B**) Bodyweights of mice surviving the treatment period of 4 weeks measured before and after treatment at the age of 4 and 8 weeks, respectively. The sample size (n) is displayed. Bars represent arithmetic means and error bars indicate 95% confidence intervals. Significant two-tailed p-values of unpaired t-tests are shown ($p < 0.05$). For the comparison between female and male mice, the respective groups were pooled prior to p-value calculation.

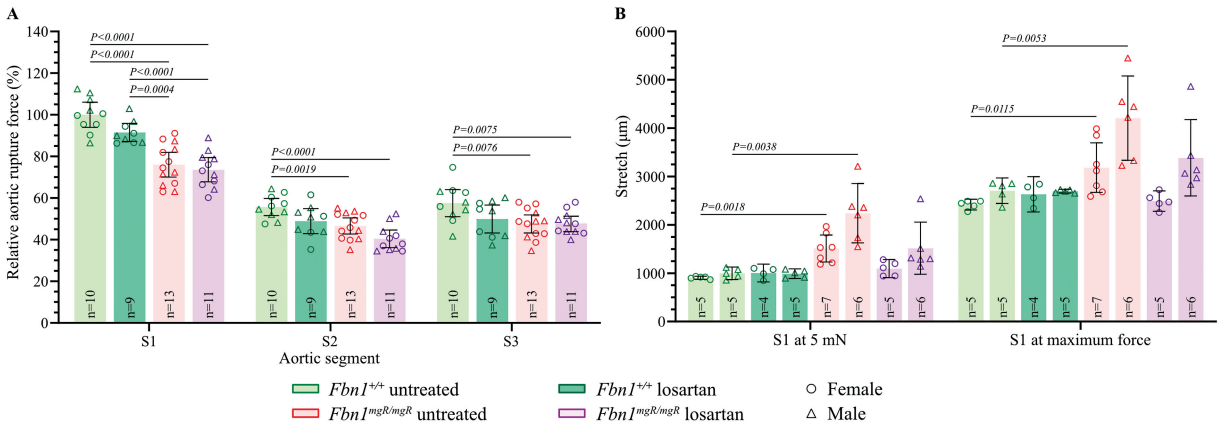

Fig. 3 Aortic parameters of the *Fbn1*^{mgR} mouse model treated with the AGTR1-inhibitor losartan. (**A**) Relative aortic rupture force (%) of three aortic segments (S1–S3) of 8-week-old *Fbn1*$^{+/+}$ and *Fbn1*$^{mgR/mgR}$ mice after 4-week-long treatment with losartan. Untreated *Fbn1*$^{+/+}$ and *Fbn1*$^{mgR/mgR}$ mice served as control. (**B**) Stretch (in µm) of the aortic segment S1 at 5 mN (load-free aortic diameter) as well as at maximum force in losartan-treated and untreated *Fbn1*$^{+/+}$ and *Fbn1*$^{mgR/mgR}$ mice separated according to sex. Bars represent arithmetic means and error bars indicate 95% confidence intervals (95% CIs). The sample size (*n*) is displayed. For mean values with non- or slightly overlapping 95% CIs compared in text, two-tailed *p*-values of unpaired *t*-tests are shown.

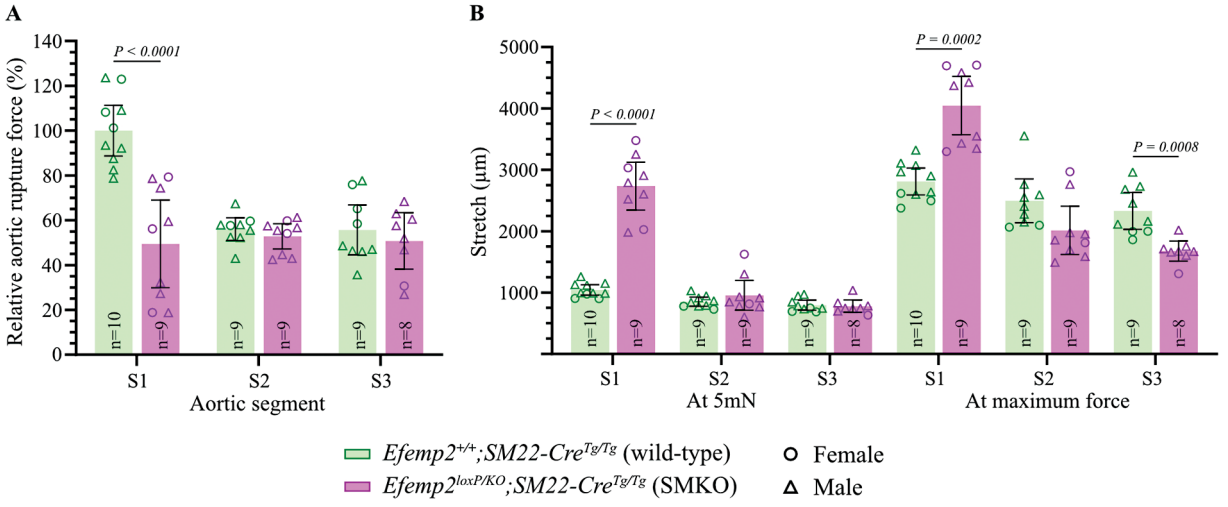

Fig. 4 Aortic parameters of the *Efemp2* SMKO mouse model. (**A**) Relative aortic rupture force (%) of three aortic segments (S1–S3) of 8-week-old wild-type and SMKO mice. (**B**) Stretch (in µm) of aortic segments at 5 mN (load-free aortic diameter) as well as at maximum force in wild-type and SMKO mice. Bars represent arithmetic means and error bars indicate 95% confidence intervals (95% CIs). The sample size (*n*) is displayed. For mean values with non- or slightly overlapping 95% CIs compared in text, two-tailed *p*-values of unpaired *t*-tests are shown.

Moreover, the rupture force of the aortic segments S1, S2, and S3 showed no considerable difference between wild-type controls and hetero-, homo-, or hemizygous mice of *Ltbp1*, *Mfap4*, and *Timp1* CRISPR/Cas9 knock-in mice (►**Fig. 5**; ►**Supplementary Table S11**, available in the online version).

Discussion

Inbred mouse hAD models are valuable tools for the investigation of medical therapeutic approaches and for the establishment of gene–disease association. Mouse hAD models have also been widely adopted for the identification of cardiovascular abnormalities by assessing aortic diameter, morphology, and wall thickness as well as by considering histological staining, omics data, or survival rate.[30–36] Although these methods provide observational insights, they cannot directly/objectively reveal at individual level how medical therapy or sequence variants influence the strength (i.e., rupture force) of the aortic wall. In this study, rupture force measurements provide individual insights into the biomechanical integrity of the thoracic aorta in three established (*Fbn1*^{C1041G}, *Fbn1*^{mgR}, and *Efemp2* SMKO) and three novel candidate-gene (*Ltbp1*, *Mfap4*, and *Timp1*) mouse hAD models.

By measuring the aortic rupture force in both mouse MFS models (i.e., the phenotypically milder heterozygous *Fbn1*^{C1041G} and the phenotypically more severe homozygous *Fbn1*^{mgR} mice), we demonstrated, to the best of our knowledge, for the first time a significant weakening of the aortic wall due to reduced rupture force values compared with wild-type littermates. Indeed, reduced rupture force is one indicator of impaired biomechanical integrity, which was

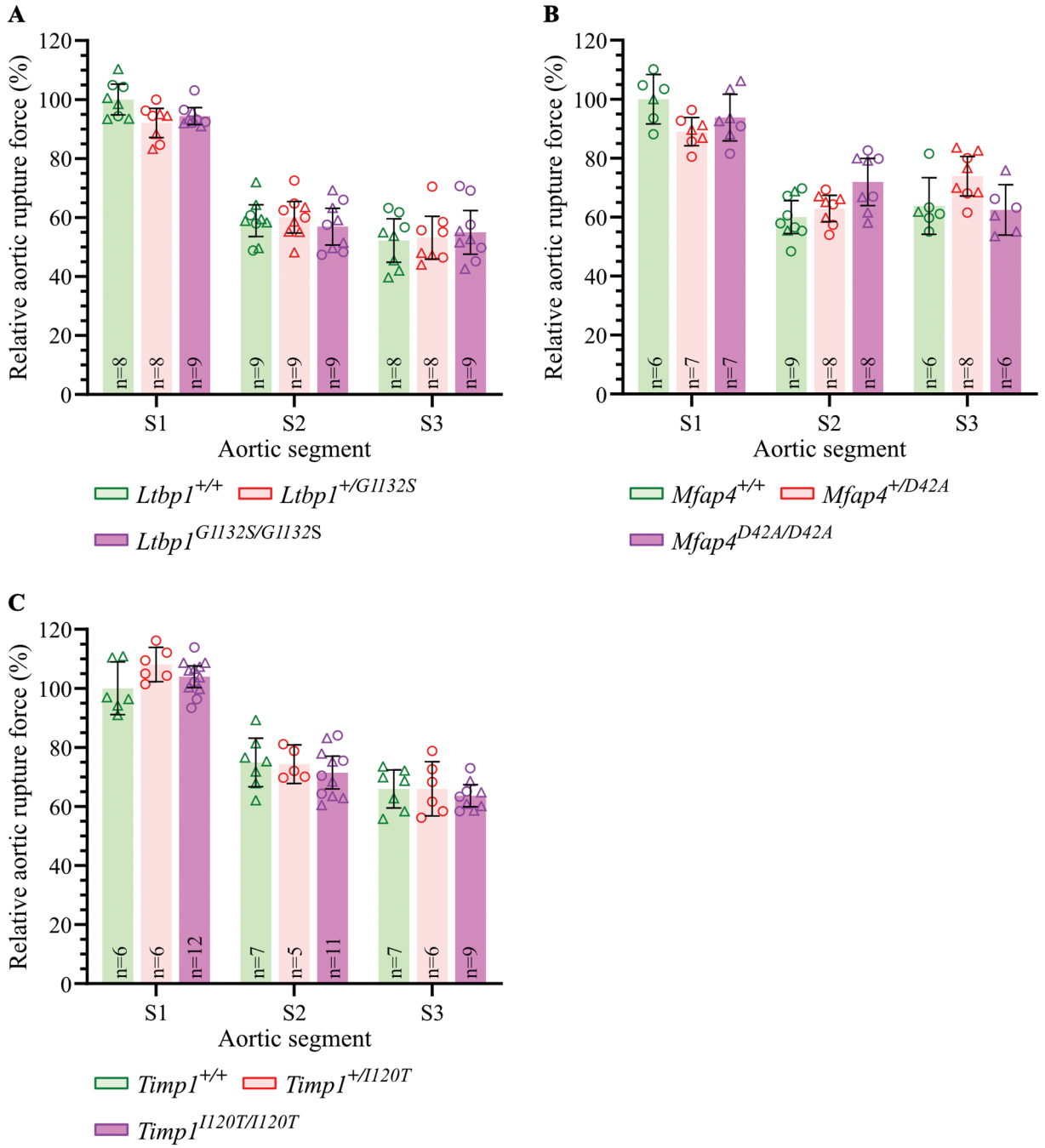

Fig. 5 Aortic rupture force of the *Ltbp1*, *Mfap4*, and *Timp1* CRISPR/Cas9 knock-in mouse models. (**A–C**) Relative aortic rupture force (%) of three aortic segments (S1–S3) of 1-year-old wild-type and hetero- as well as hemi- and homozygous *Ltbp1* (A), *Mfap4* (B), and *Timp1* (C) CRISPR/Cas9 knock-in mice. Bars represent arithmetic means, error bars indicate 95% confidence intervals (95% CIs). The sample size (*n*) is displayed. Note the absence of non- or slightly overlapping 95% CIs per aortic segment. Circle, female; triangle, male.

most noticeably present in the ascending aorta (S1 in ►**Figs. 1A** and **3A**). However, since both MFS mouse models showed a comparable reduction in rupture force, although *Fbn1*$^{mgR/mgR}$ mice are more prone to die from spontaneous aortic rupture, neither aortic rupture force nor genotype alone is sufficient for fatal aortic events. The aortic wall of *Fbn1*$^{+/C1041G}$ mice is known to be normal in (histological) appearance until approximately 2 months of age, but thereafter medial thickening and/or progressive deterioration within the medial layer, including fragmentation of elastic fibers, may be observed.[17] As *Fbn1*$^{+/C1041G}$ mice used in this study were 10 weeks (2.3 months) old, our read-out system can detect impaired aortic wall integrity at an early stage of progressive aortic wall damage and before the development of aortic aneurysms.

Compared with wild-type controls and in contrast to *Fbn1*$^{+/C1041G}$ mice, the ascending aorta of *Fbn1*$^{mgR/mgR}$ mice showed significantly increased stretch at both 5 mN and maximum force (cf. ►**Figs. 1B** and **3B**; ►**Supplementary Fig. S3B**, available in the online version); note that the stretch

of ring-shaped S1–S3 reflects half the circumference of the aorta and thus the aortic diameter). Increased aortic stretch was even more pronounced in male than in female mice, which is in line with previously published aortic diameters using ultrasound measurements.[37,38] Indeed, sex is a well-known risk factor for cardiovascular diseases and several clinical studies have shown that sex also strongly influences the outcome of MFS, with men having a higher risk for aortic dilatations and other arterial events.[39–41]

In addition, the antihypertensive drug losartan recognizably reduced S1 stretch, which reflects aortic diameter, but had no impact on S1–S3 rupture force in *Fbn1*$^{mgR/mgR}$ mice (►**Fig. 3**; ►**Supplementary Fig. S3B**, available in the online version), implying that the thoracic aorta treated with losartan remains susceptible to rupture despite the reduction in aortic stretch/diameter. Further studies are needed to clarify the reason for this incomplete effect of losartan, such as (1) reduction of aortic wall stress by lowering blood pressure load/spikes, (2) blood pressure-independent reduction of aortic dilatation by improving elastic properties, but not biomechanical integrity, of the thoracic (ascending) aortic wall, or (3) the time dependence of the treatment.[42–44] For example, it is possible that losartan treatment could impact rupture force if the treatment had lasted longer and/or a different time point in the disease process was evaluated. Nevertheless, aortic rupture force, beyond aortic diameter, may be useful for the investigation of potential drug therapies in mouse models of hAD characterized by aneurysms. We propose that our read-out system provides clinically relevant information allowing novel insights into the evaluation of medical therapies for the prevention of arterial events in hADs that cannot be obtained by assessment of the aortic diameter alone.

In the *Efemp2* SMKO mouse model, our data show that the absence of Fbln4 in the aortic ECM results in significantly reduced rupture force and increased stretch of the ascending aorta, indicating impaired biomechanical integrity of the aortic wall (►**Figs. 4**; ►**Supplementary Fig. S3C**, available in the online version). This is likely related to the effect of Fbln4 on elastogenesis[45] and collagen biosynthesis[26] involved in the development of ascending aortic aneurysms,[46,47] as previously described. Considering that the ascending aorta is subjected to the highest hemodynamic stress, it is not surprising that knockout of *Efemp2* in vascular smooth muscle cells has a stronger effect on the ascending than on the descending aorta (i.e., S1 compared with S2 and S3), despite the higher elastin content of the ascending aorta.[48,49]

Compared with the previously reported *Col3a1*^{m1Lsmi} mouse vEDS model,[12,16] the aortic rupture forces of both *Fbn1*$^{+/C1041G}$ and *Fbn1*$^{mgR/mgR}$ mouse MFS models were significantly higher in all three aortic segments (►**Fig. 6**;

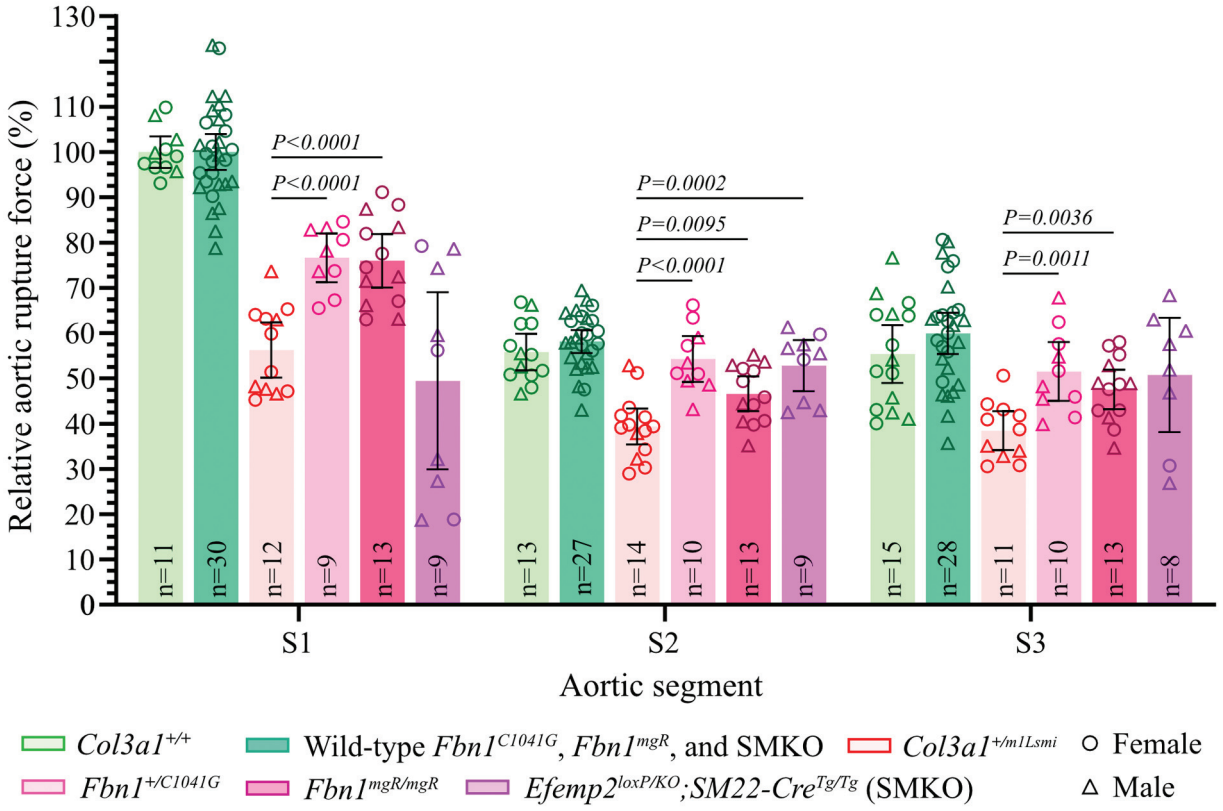

Fig. 6 Aortic rupture force of the *Fbn1*^{C1041G}, *Fbn1*^{mgR}, and *Efemp2* SMKO mouse models compared with *Col3a1*^{m1Lsmi} mice modeling vEDS. Relative aortic rupture force (%) of three aortic segments (S1–S3) of the mouse models *Col3a1*^{m1Lsmi} (data as described previously),[12] *Fbn1*^{C1041G}, *Fbn1*^{mgR}, and *Efemp2* SMKO (cf. wild-type controls of the *Fbn1*^{C1041G}, *Fbn1*^{mgR}, and *Efemp2* SMKO mouse models were pooled). Bars represent arithmetic means, error bars indicate 95% confidence intervals (95% CIs). The sample size (*n*) is displayed. For mean values with non- or slightly overlapping 95% CIs compared in text, two-tailed *p*-values of unpaired *t*-tests are shown. *Col3a1*$^{+/+}$ and *Col3a1*$^{+/m1Lsmi}$ denote wild-type and heterozygous mice of the *Col3a1*^{m1Lsmi} mouse model, respectively.

►**Supplementary Table S12**, available in the online version). This relative aortic weakness of the *Col3a1*$^{+/m1Lsmi}$ mice is consistent with their higher mortality rate compared with *Fbn1*$^{mgR/mgR}$ mice (►**Supplementary Fig. S4**, available in the online version; note that survival rate does not reflect aortic rupture force at the individual level, as not all mice with significantly reduced rupture force showed reduced survival). In contrast, SMKO mice showed in the ascending aorta (S1) relative aortic rupture force values comparable to or lower than those of mice modeling vEDS, but in the descending aorta (S2 and S3) the relative rupture force of SMKO mice was comparable to that of mice modeling MFS (►**Fig. 6**; ►**Supplementary Table S12**, available in the online version).

Given that our measurements demonstrated reduced aortic rupture force of established hAD mouse models in this study (*Fbn1*^{C1041G}, *Fbn1*^{mgR}, and *Efemp2* SMKO) and elsewhere (*Col3a1*^{m1Lsmi}),[12,16] we also evaluated aortic rupture force in three CRISPR/Cas9-engineered mouse models of hAD candidate genes. In humans, these three genes (*LTBP1*, *MFAP4*, and *TIMP1*) are expressed at higher levels in arterial tissue than in any other tissue studied in GTEx (gtexportal.org/home). LTBP1 interacts with ECM proteins, such as MFS-associated FBN1, and regulates transforming growth factor (TGF)-β,[50] which plays an important role in the pathogenesis of hADs.[51] MFAP4, an ECM protein found in elastic fibers, interacts with FBN1, FBN2, and type I collagen as well as actively promotes tropoelastin self-assembly by binding tropoelastin.[52] TIMP1 is a strong inhibitor of many MMPs, thereby preventing excessive ECM degradation.[53] Knockout mouse models of *Ltbp1*, *Mfap4*, and *Timp1* showed cardiovascular phenotypes,[54–59] indicating that mutations in these genes could be the cause of hAD.

In contrast to established hAD mouse models (i.e., mice with mutation in the genes *Fbn1*, *Efemp2*, or *Col3a1*), however, our read-out system revealed no significantly reduced aortic rupture force for any genotypes of the three novel knock-in mouse models *Ltbp1*^{G1132S}, *Mfap4*^{D42A}, and *Timp1*^{I120T} at the age of 1 year (►**Fig. 5**). This indicates and clarifies the lack of aortic significance of the human-equivalent sequence variants with unknown pathogenicity knocked into our mouse models. The nonreduced aortic rupture forces of the three knock-in mouse models are consistent with their nonincreased aortic stretch and nonreduced survival rate (data not shown). Further studies are needed to assess the clinical significance of the genes *LTBP1*, *MFAP4*, and *TIMP1* in hAD, also considering a disease-modifying (synergistic) effect of these genes as well as mice with a different genetic background.[60]

Taken together, this study demonstrates that the measurement of aortic rupture force can not only explain the aortic phenotype of established mouse hAD models but also clarify the unknown/uncertain aortic significance of candidate genes, variants, and drugs, thereby paving the way for better molecular diagnosis and medical therapies in hAD. Thus, rupture force can be a valuable parameter to consider in future studies of aortic aneurysms and dissections, especially in evaluating the beneficial effects of pharmacological therapies to attenuate the risk of these life-threatening conditions.

What is known about this topic?

- Hereditary aortic diseases (hADs) can lead to aneurysms, dissections, and ruptures, depending on the genetic cause, blood pressure load, age, and other factors weakening the aortic wall.
- Biomechanical properties of hADs and drug treatments of aortic weakness remain understudied.
- Methods with objective read-out are required that can assess aortic-wall weakness at an individual level even in the absence of arterial events.

What does this paper add?

- In mice modeling the hAD Marfan syndrome, losartan treatment reduced thoracic aortic aneurysm formation without affecting aortic rupture strength, and the measurement of aortic rupture force showed weakened thoracic aorta prior to micro- and macroscopic changes.
- Smooth-muscle-cell-knockout of Efemp2 significantly impaired the rupture force of the murine ascending aorta.
- Aortic rupture force measurements could also clarify the causality of candidate gene(s)/variant(s) in mouse models of aortic diseases.

Funding
This work was supported by the Isaac Dreyfus-Bernheim Stiftung and the Fondation pour la Recherche et le Traitement Médical (FRTM) as well as by National Institutes of Health NHLBI (grant number K01 HL149984) and JSPS KAKENHI (grant number JP20H03762).

Conflict of Interest
None declared.

Acknowledgment
We thank Cyagen (Santa Clara, California, United States) for help with the generation of the three CRISPR/Cas9 knock-in mouse models, Bryana M. Levitan for performing ultrasound measurements of *Fbn1*^{mgR} mice as well as Daniela Brkan, Edina Jusufi, Marc T. Schönholzer, Giancarlo Tomio, and Dzenneta Zukovic for help with data analysis and/or figure preparation.

References

1 Lindsay ME, Dietz HC. Lessons on the pathogenesis of aneurysm from heritable conditions. Nature 2011;473(7347):308–316
2 Verstraeten A, Luyckx I, Loeys B. Aetiology and management of hereditary aortopathy. Nat Rev Cardiol 2017;14(04):197–208

3 Creamer TJ, Bramel EE, MacFarlane EG. Insights on the pathogenesis of aneurysm through the study of hereditary aortopathies. Genes (Basel) 2021;12(02):183
4 Caspar SM, Dubacher N, Kopps AM, Meienberg J, Henggeler C, Matyas G. Clinical sequencing: from raw data to diagnosis with lifetime value. Clin Genet 2018;93(03):508–519
5 Renard M, Francis C, Ghosh R, et al. Clinical validity of genes for heritable thoracic aortic aneurysm and dissection. J Am Coll Cardiol 2018;72(06):605–615
6 Caspar SM, Dubacher N, Matyas G. More genes for thoracic aortic aneurysms and dissections. J Am Coll Cardiol 2019;73(04): 528–529
7 Humphrey JD, Milewicz DM, Tellides G, Schwartz MA. Cell biology. Dysfunctional mechanosensing in aneurysms. Science 2014; 344(6183):477–479
8 Humphrey JD, Schwartz MA, Tellides G, Milewicz DM. Role of mechanotransduction in vascular biology: focus on thoracic aortic aneurysms and dissections. Circ Res 2015;116(08):1448–1461
9 Pierce DM, Maier F, Weisbecker H, et al. Human thoracic and abdominal aortic aneurysmal tissues: damage experiments, statistical analysis and constitutive modeling. J Mech Behav Biomed Mater 2015;41:92–107
10 Chiu P, Lee H-P, Dalal AR, et al. Relative strain is a novel predictor of aneurysmal degeneration of the thoracic aorta: an ex vivo mechanical study. JVS Vasc Sci 2021;2:235–246
11 Chittajallu SNSH, Richhariya A, Tse KM, Chinthapenta V. A review on damage and rupture modelling for soft tissues. Bioengineering (Basel) 2022;9(01):26
12 Dubacher N, Münger J, Gorosabel MC, et al. Celiprolol but not losartan improves the biomechanical integrity of the aorta in a mouse model of vascular Ehlers-Danlos syndrome. Cardiovasc Res 2020;116(02):457–465
13 Ong K-T, Perdu J, De Backer J, et al. Effect of celiprolol on prevention of cardiovascular events in vascular Ehlers-Danlos syndrome: a prospective randomised, open, blinded-endpoints trial. Lancet 2010;376(9751):1476–1484
14 Frank M, Adham S, Seigle S, et al. Vascular Ehlers-Danlos syndrome: Long-term observational study. J Am Coll Cardiol 2019;73 (15):1948–1957
15 Baderkhan H, Wanhainen A, Stenborg A, Stattin E-L, Björck M. Celiprolol treatment in patients with vascular Ehlers-Danlos syndrome. Eur J Vasc Endovasc Surg 2021;61(02):326–331
16 Gorosabel MC, Dubacher N, Meienberg J, Matyas G. Vascular Ehlers-Danlos syndrome: can the beneficial effect of celiprolol be extrapolated to bisoprolol? Eur Heart J Cardiovasc Pharmacother 2020;6(03):199–200
17 Judge DP, Biery NJ, Keene DR, et al. Evidence for a critical contribution of haploinsufficiency in the complex pathogenesis of Marfan syndrome. J Clin Invest 2004;114(02):172–181
18 Pereira L, Lee SY, Gayraud B, et al. Pathogenetic sequence for aneurysm revealed in mice underexpressing fibrillin-1. Proc Natl Acad Sci U S A 1999;96(07):3819–3823
19 Bunton TE, Biery NJ, Myers L, Gayraud B, Ramirez F, Dietz HC. Phenotypic alteration of vascular smooth muscle cells precedes elastolysis in a mouse model of Marfan syndrome. Circ Res 2001; 88(01):37–43
20 Saeyeldin A, Zafar MA, Velasquez CA, et al. Natural history of aortic root aneurysms in Marfan syndrome. Ann Cardiothorac Surg 2017;6(06):625–632
21 Habashi JP, Judge DP, Holm TM, et al. Losartan, an AT1 antagonist, prevents aortic aneurysm in a mouse model of Marfan syndrome. Science 2006;312(5770):117–121
22 Habashi JP, Doyle JJ, Holm TM, et al. Angiotensin II type 2 receptor signaling attenuates aortic aneurysm in mice through ERK antagonism. Science 2011;332(6027):361–365
23 Bhatt AB, Buck JS, Zuflacht JP, et al. Distinct effects of losartan and atenolol on vascular stiffness in Marfan syndrome. Vasc Med 2015;20(04):317–325
24 Cook JR, Clayton NP, Carta L, et al. Dimorphic effects of transforming growth factor-β signaling during aortic aneurysm progression in mice suggest a combinatorial therapy for Marfan syndrome. Arterioscler Thromb Vasc Biol 2015;35(04):911–917
25 Robertson DM, Truong DT, Cox DA, et al. Pediatric Heart Network trial of losartan vs. atenolol in children and young adults with Marfan syndrome: impact on prescription practices. Pediatr Cardiol 2023;44(03):618–623
26 Huang J, Davis EC, Chapman SL, et al. Fibulin-4 deficiency results in ascending aortic aneurysms: a potential link between abnormal smooth muscle cell phenotype and aneurysm progression. Circ Res 2010;106(03):583–592
27 Hucthagowder V, Sausgruber N, Kim KH, Angle B, Marmorstein LY, Urban Z. Fibulin-4: a novel gene for an autosomal recessive cutis laxa syndrome. Am J Hum Genet 2006;78(06):1075–1080
28 Renard M, Holm T, Veith R, et al. Altered TGFbeta signaling and cardiovascular manifestations in patients with autosomal recessive cutis laxa type I caused by fibulin-4 deficiency. Eur J Hum Genet 2010;18(08):895–901
29 Muthu ML, Tiedemann K, Fradette J, Komarova S, Reinhardt DP. Fibrillin-1 regulates white adipose tissue development, homeostasis, and function. Matrix Biol 2022;110:106–128
30 Lee VS, Halabi CM, Hoffman EP, et al; Brigham Genomic Medicine. Loss of function mutation in LOX causes thoracic aortic aneurysm and dissection in humans. Proc Natl Acad Sci U S A 2016;113(31): 8759–8764
31 Halabi CM, Broekelmann TJ, Lin M, Lee VS, Chu M-L, Mecham RP. Fibulin-4 is essential for maintaining arterial wall integrity in conduit but not muscular arteries. Sci Adv 2017;3(05):e1602532
32 Parker SJ, Stotland A, MacFarlane E, et al. Proteomics reveals Rictor as a noncanonical TGF-β signaling target during aneurysm progression in Marfan mice. Am J Physiol Heart Circ Physiol 2018;315 (05):H1112–H1126
33 Bhushan R, Altinbas L, Jäger M, et al. An integrative systems approach identifies novel candidates in Marfan syndrome-related pathophysiology. J Cell Mol Med 2019;23(04):2526–2535
34 Bowen CJ, Calderón Giadrosic JF, Burger Z, et al. Targetable cellular signaling events mediate vascular pathology in vascular Ehlers-Danlos syndrome. J Clin Invest 2020;130(02):686–698
35 Xiong W, Meisinger T, Knispel R, Worth JM, Baxter BT. MMP-2 regulates Erk1/2 phosphorylation and aortic dilatation in Marfan syndrome. Circ Res 2012;110(12):e92–e101
36 Daugherty A, Sawada H, Sheppard MB, Lu HS. Angiotensinogen as a therapeutic target for cardiovascular and metabolic diseases. Arterioscler Thromb Vasc Biol 2024;44(05):1021–1030
37 Chen JZ, Sawada H, Ye D, et al. Deletion of AT1a (Angiotensin II Type 1a) receptor or inhibition of angiotensinogen synthesis attenuates thoracic aortopathies in Fibrillin1$^{C1041G/+}$ mice. Arterioscler Thromb Vasc Biol 2021;41(10):2538–2550
38 Chen JZ, Sawada H, Moorleghen JJ, Weiland M, Daugherty A, Sheppard MB. Aortic strain correlates with elastin fragmentation in fibrillin-1 hypomorphic mice. Circ Rep 2019;1(05):199–205
39 Détaint D, Faivre L, Collod-Beroud G, et al. Cardiovascular manifestations in men and women carrying a FBN1 mutation. Eur Heart J 2010;31(18):2223–2229
40 Holmes KW, Maslen CL, Kindem M, et al; GenTAC Registry Consortium. GenTAC registry report: gender differences among individuals with genetically triggered thoracic aortic aneurysm and dissection. Am J Med Genet A 2013;161A(04):779–786
41 Renard M, Muiño-Mosquera L, Manalo EC, et al. Sex, pregnancy and aortic disease in Marfan syndrome. PLoS One 2017;12(07):e0181166
42 Cassis LA, Gupte M, Thayer S, et al. ANG II infusion promotes abdominal aortic aneurysms independent of increased blood pressure in hypercholesterolemic mice. Am J Physiol Heart Circ Physiol 2009;296(05):H1660–H1665
43 Sun Y, Asano K, Sedes L, et al. Dissecting aortic aneurysm in Marfan syndrome is associated with losartan-sensitive transcriptomic modulation of aortic cells. JCI Insight 2023;8(10):e168793

44 Seeburun S, Wu S, Hemani D, et al. Insights into elastic fiber fragmentation: Mechanisms and treatment of aortic aneurysm in Marfan syndrome. Vascul Pharmacol 2023;153:107215
45 Horiguchi M, Inoue T, Ohbayashi T, et al. Fibulin-4 conducts proper elastogenesis via interaction with cross-linking enzyme lysyl oxidase. Proc Natl Acad Sci U S A 2009;106(45):19029–19034
46 Papke CL, Yanagisawa H. Fibulin-4 and fibulin-5 in elastogenesis and beyond: insights from mouse and human studies. Matrix Biol 2014;37:142–149
47 Papke CL, Tsunezumi J, Ringuette L-J, et al. Loss of fibulin-4 disrupts collagen synthesis and maturation: implications for pathology resulting from EFEMP2 mutations. Hum Mol Genet 2015;24(20):5867–5879
48 Ruddy JM, Jones JA, Spinale FG, Ikonomidis JS. Regional heterogeneity within the aorta: relevance to aneurysm disease. J Thorac Cardiovasc Surg 2008;136(05):1123–1130
49 Jana S, Hu M, Shen M, Kassiri Z. Extracellular matrix, regional heterogeneity of the aorta, and aortic aneurysm. Exp Mol Med 2019;51(12):1–15
50 Morisaki T, Morisaki H. Genetics of hereditary large vessel diseases. J Hum Genet 2016;61(01):21–26
51 Neptune ER, Frischmeyer PA, Arking DE, et al. Dysregulation of TGF-beta activation contributes to pathogenesis in Marfan syndrome. Nat Genet 2003;33(03):407–411
52 Pilecki B, Holm AT, Schlosser A, et al. Characterization of microfibrillar-associated protein 4 (MFAP4) as a tropoelastin- and fibrillin-binding protein involved in elastic fiber formation. J Biol Chem 2016;291(03):1103–1114
53 Brew K, Nagase H. The tissue inhibitors of metalloproteinases (TIMPs): an ancient family with structural and functional diversity. Biochim Biophys Acta 2010;1803(01):55–71
54 Roten L, Nemoto S, Simsic J, et al. Effects of gene deletion of the tissue inhibitor of the matrix metalloproteinase-type 1 (TIMP-1) on left ventricular geometry and function in mice. J Mol Cell Cardiol 2000;32(01):109–120
55 Eskandari MK, Vijungco JD, Flores A, Borensztajn J, Shively V, Pearce WH. Enhanced abdominal aortic aneurysm in TIMP-1-deficient mice. J Surg Res 2005;123(02):289–293
56 Todorovic V, Frendewey D, Gutstein DE, et al. Long form of latent TGF-beta binding protein 1 (Ltbp1L) is essential for cardiac outflow tract septation and remodeling. Development 2007; 134(20):3723–3732
57 Todorovic V, Finnegan E, Freyer L, Zilberberg L, Ota M, Rifkin DB. Long form of latent TGF-β binding protein 1 (Ltbp1L) regulates cardiac valve development. Dev Dyn 2011;240(01):176–187
58 Schlosser A, Pilecki B, Hemstra LE, et al. MFAP4 promotes vascular smooth muscle migration, proliferation and accelerates neointima formation. Arterioscler Thromb Vasc Biol 2016;36(01): 122–133
59 Arpino V, Brock M, Gill SE. The role of TIMPs in regulation of extracellular matrix proteolysis. Matrix Biol 2015;44-46:247–254
60 Ritskes-Hoitinga M, Leenaars C, Beumer W, Coenen-de Roo T, Stafleu F, Meijboom FLB. Improving translation by identifying evidence for more human-relevant preclinical strategies. Animals (Basel) 2020;10(07):1170

